Cross-section measurements of capture reactions relevant to the p process using a 4π γ-summing method

A. Spyrou,[1] H.-W. Becker,[2] A. Lagoyannis,[1] S. Harissopulos,[1,*] and C. Rolfs[2]
[1]*Institute of Nuclear Physics, NCSR "Demokritos," GR-153.10 Aghia Paraskevi, Athens, Greece*
[2]*DTL, Institut für Experimentalphysik III, Ruhr-Universität Bochum, Universitatsstrasse 150, D-40781 Bochum, Germany*
(Received 27 September 2006; revised manuscript received 29 May 2007; published 23 July 2007)

A new method employing a 12 inch × 12 inch γ-summing single NaI crystal was developed for cross-section measurements of astrophysically relevant capture reactions on medium-mass nuclei. The response function of such a 4π detector enables the summing of all capture events. As a result, a single peak, the so-called sum peak, arises in the spectra. Its intensity can be used to obtain cross sections of capture reactions with unknown multiplicities. The method enables to first determine these multiplicities, which are then used to derive the corresponding efficiency of the sum peak by means of Monte Carlo simulations. Cross sections are finally obtained from the sum-peak intensity with an average uncertainty of ≈15%. The method was first applied to the ^{62}Ni$(\alpha,\gamma)^{66}$Zn reaction. The results obtained are in excellent agreement with those reported in literature. The new method proposed here was then employed to determine cross sections of 25 capture reactions in the Ni–Sb region. The cross sections measured for the ^{103}Rh$(p,\gamma)^{104}$Pd reaction are also presented. A very good agreement between the cross sections measured in the present work and the corresponding predictions of the Hauser-Feshbach theory was found.

DOI: 10.1103/PhysRevC.76.015802 PACS number(s): 25.55.−e, 25.40.Lw, 24.60.Dr, 29.40.Mc

I. MOTIVATION

Cross-section measurements of capture reactions are by far the major task in experimental nuclear astrophysics. All too often, however, this task is not a simple one as most of the cross sections desired to be determined are in the μb range or even below. So far, various experimental setups have been applied for this purpose and the success of the measurements has strongly depended on (i) the high efficiency of the detectors used, (ii) the low beam-induced background, and (iii) the quality and stability of the targets employed.

The two former conditions are quite reasonably satisfied in the case of measurements with the activation technique [1]. Hereby, the energy of the γ rays to be detected off-line ranges, in most of the studied cases, between 100 keV and 2 MeV. Hence, small-size single-crystal Ge detectors with typical relative efficiencies of ≈20–30% can be employed to determine γ activities and derive cross sections. In addition, the γ spectra are usually free from beam-induced background because they are accumulated off-line after the irradiation of the target. In some cases, however, the target irradiation produces intense and often long-lived β activities, which result in a very strong 511-keV γ line that loads the γ spectra with a high Compton background. As a result, γ transitions with energies below 500 keV are strongly "obscured" by the Compton continuum. To overcome this problem, Ge detectors have to be shielded with bismuth germanate crystals (BGO) to suppress the Compton events. The fact that one can use natural targets, in combination with the aforementioned simple setup requirements, makes the activation technique a straightforward procedure and therefore the method applied the most provided the reaction of interest leads to an unstable nucleus with a suitable half-life. The latter constraint does not apply in the case of in-beam cross-section measurements where any reaction can be investigated in principal. In a capture reaction the total cross section σ_T is derived from the total reaction yield Y by using

$$\sigma_T = \frac{A}{N_A}\frac{Y}{\xi}, \tag{1}$$

where A is the atomic weight in *amu* of the target used, N_A is the Avogadro number, and ξ is the target thickness.

The total reaction yield Y can be extracted from the absolute intensities of all the *primary* γ transitions, i.e., those depopulating the entry state of the produced compound nucleus. In the simplified case shown in Fig. 1, these transitions are labeled γ_0, γ_1, and γ_2. Their absolute γ intensities are obtained from the absolute efficiency corrected A_0 coefficients of the corresponding angular distributions. In practice, the total cross section is determined from the angular distributions of the γ transitions feeding the ground state and not from those of the primary γ rays (see, e.g, in Ref. [2]). Hence, the total reaction yield Y is deduced from

$$Y = \sum_i^N A_0^i, \tag{2}$$

where N is the total number of the γ transitions feeding the ground state. Obviously the determination of cross sections from γ-angular distribution measurements can become very time-consuming with increasing number N of γ transitions, because the number of γ spectra that have to be accumulated and subsequently analyzed at each energy is usually $5N$ at least (see, e.g., in Ref. [2] where $N = 12$). A crucial point in this method is the determination of the absolute intensity of the γ_0 transition. Though its intensity may be a small fraction of the total reaction yield, e.g., at most 5%, it cannot be neglected

*sharisop@inp.demokritos.gr

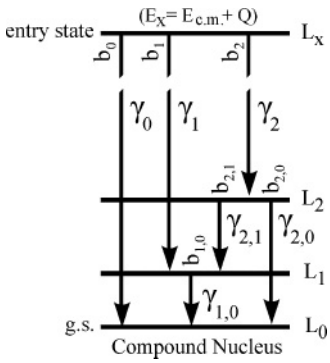

FIG. 1. Simplified decay scheme of a compound nucleus produced in a capture reaction at an excited (entry) state with energy E_X. The levels of the compound nucleus are labeled L_0 (ground state), L_1 (1st excited state), L_2 (2nd excited state), and L_X (entry state). The branchings of the primary γ transitions to the ground, first, and second excited states are labeled b_0, b_1, and b_2, respectively. The branchings of the secondary γ rays are labeled $b_{i,f}$, where i is the i-th excited initial state and f is the f-th excited final level. For the decay scheme shown, it obviously holds that $i > f$ and $b_{1,0} = 100\%$.

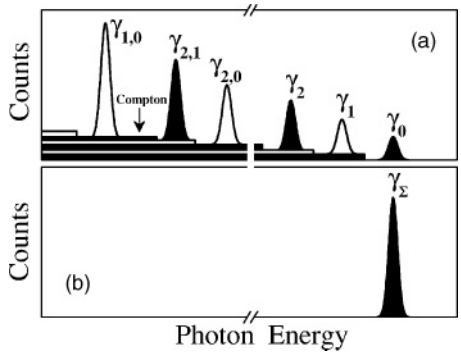

FIG. 2. Typical γ spectra expected for the de-excitation of the compound nucleus illustrated in Fig. 1 by using (i) a small-size NaI(Tl) crystal and (ii) a large volume 4π NaI(Tl) summing detector.

a priori. This sets certain requirements for the efficiency of the setup to be used, because the energy E_{γ_0} of γ_0 can be very high, as it is equal to the sum of the center-of-mass energy (c.m.) and the Q value of the reaction, i.e., $E_{\gamma_0} = E_{\text{c.m.}} + Q$. In the case of proton or α-particle capture reactions, E_{γ_0} often exceeds 8 MeV. Consequently, the determination of the absolute intensity of γ_0 requires a very efficient setup, preferably an array of large-volume HPGe detectors of almost 100% relative efficiency with BGO shields for Compton suppression like the one employed in Ref. [2]. The situation becomes simpler when all capture events are "gathered" in only one excited level, i.e., when the relevant γ cascades feed only one state, most likely the first excited state, which is then de-excited to the ground state by a single γ transition. In this case, only the latter γ transition needs to be analyzed, as demonstrated in Ref. [3].

Finally, in-beam measurements of γ-angular distributions may also suffer from an additional problem, i.e., the beam-induced background, especially when light elements are present as admixtures in the backing or even in the target material. The use of α beams causes additional problems because, in most of the cases, the (α, n) reaction channel is open. This channel is stronger by at least one to three orders of magnitude compared to the corresponding (α, γ) reaction of interest.

The need for an extended data base of capture reaction cross sections relevant to the modeling of the nucleosynthetic p process [4] motivated us to exploit an alternative method for cross-section measurements that enables us to study any reaction within relatively short beam times. This method is based on in-beam measurements of angle-integrated γ fluxes and it was first realized by employing a large-volume eightfold segmented NaI(Tl) crystal as we already described in Ref. [5]. Meanwhile, the method has been improved by utilizing a 12×12 inch single NaI(Tl) crystal that is presented here. The principles of this 4π γ-summing method are outlined in Sec. II. The setup used in the present work is described in Sec. III. The experimental procedures applied in the present work and the cross-section results obtained are presented in Secs. IV and V, respectively. The conclusions are finally summarized in Sec. VI.

II. THE 4π γ-SUMMING METHOD

The proposed method is based on the use of a large-volume NaI(Tl) detector covering a solid angle of almost 4π for photons emitted by a target placed at its center. The working principle of such a detector relies on its long time response and its large volume. The latter enables to fully absorb a photon, whereas the former renders the photomultipliers unable to distinguish between different photons emitted within a time interval smaller than the decay time of the crystal, which is typically $\gtrsim$250 ns. As a result, the corresponding photons give one common signal corresponding to an energy equal to the sum of their individual energies.

Because of these features, a spectrum measured with a large-volume NaI(Tl) crystal differs significantly from that measured with a small-size one. The differences are illustrated in Fig. 2. The spectrum shown in part (a) is a sketch of a typical γ spectrum measured with a small-size NaI(Tl) crystal for the deexcitation of the compound nucleus in the simple case shown in Fig. 1. The spectrum includes the γ_0, γ_1, γ_2, $\gamma_{2,1}$, $\gamma_{2,0}$, and $\gamma_{1,0}$ transitions as well as their accompanying Compton continuum. In contrast, the spectrum displayed in part (b) is that expected for an appropriately large NaI(Tl) detector. Hereby, photons have been fully absorbed so that no Compton continuum appears. Moreover, the six peaks shown in part (a) have been "replaced" by one peak, which is located at an energy E_Σ equal to that of the γ_0 transition. Its intensity I_Σ, however, is higher than the one of γ_0 because it results from the summation of γ_0 with the three different γ cascades formed by the sequential photons γ_1 and $\gamma_{1,0}$ in the first case, γ_2, $\gamma_{2,1}$, and $\gamma_{1,0}$ in the second, and γ_2 and $\gamma_{2,0}$ in the third one.

It becomes thus clear that the main advantage in using a large-volume 4π summing detector is that instead of measuring at least five γ spectra at each beam energy and further analyzing numerous γ transitions, one needs to acquire only one spectrum and analyze only one γ peak, the so-called

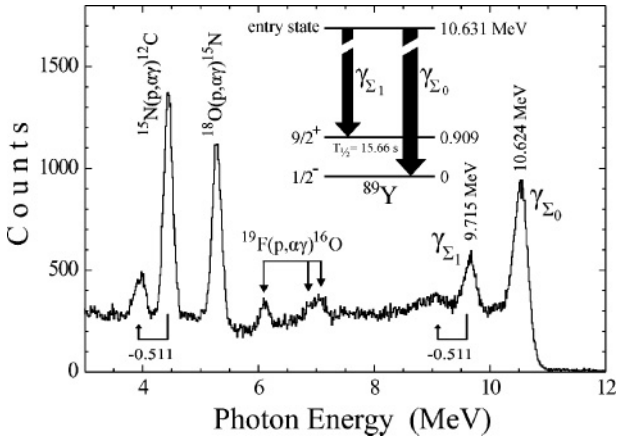

FIG. 3. γ-singles spectrum measured in the present work for the ^{88}Sr$(p,\gamma)^{89}$Y reaction at $E_p = 3.6$ MeV. The target was produced by evaporating ^{88}Sr$(NO_3)_2$ on a 0.2-mm-thick Ta foil [2] (see also text).

sum peak. Its intensity I_Σ can be used to determine the total reaction yield Y from

$$Y = \frac{I_\Sigma}{N_b \varepsilon_\Sigma}, \tag{3}$$

where N_b is the number of the beam particles and ε_Σ is the sum-peak efficiency. The total cross section σ_T is then derived by inserting Y in Eq. (1). Apparently, because of the 4π geometry covered by the summing crystal, corrections for angular distribution effects are not necessary.

The "ideal" spectrum shown in part (b) of Fig. 2 is, however, quite different from what is measured in "real" experiments: Spectra do not consist of just a single peak, because some photons are not fully absorbed and the Compton continuum as well as individual peaks also appear. In addition, the spectra may include more than one sum peak when the compound nucleus of interest has excited levels depopulated via $E0$ transitions or have half-lives longer than the decay time of the NaI crystal. The latter case is demonstrated by the spectrum displayed in Fig. 3. This spectrum was measured with the summing detector employed in the present work (see next section). It includes two sum peaks located at 10.624 and 9.715 MeV that are labeled γ_{Σ_0} and γ_{Σ_1}, respectively. They both belong to ^{89}Y that is produced by the ^{88}Sr$(p,\gamma)^{89}$Y reaction at $E_p = 3.6$ MeV. The first sum peak is the result of the sum of the γ_0 transition from the entry state and all the γ cascades by-passing the first excited level, which is located at an excitation energy of 0.909 MeV as indicated in the level scheme shown in Fig. 3, and feeding the ground state. The energy of γ_{Σ_0} is slightly lower than $E_{\text{c.m.}} + Q = 10.631$ MeV due to the energy loss of the proton beam in the target material. The energy of γ_{Σ_1} is 0.909 MeV lower than that of γ_{Σ_0} because it corresponds to the sum of the γ cascades de-exciting the entry state and feeding the first excited state of ^{89}Y. The latter $9/2^+$ level has a half-life of 15.66 s that is considerably longer than the decay time of the NaI(Tl) crystal.

In addition to the two sum peaks, the spectrum of Fig. 3 also includes peaks from reactions of the proton beam with ^{18}O and ^{15}N. These nuclei are present as admixtures in the target because the latter was produced by evaporation of ^{88}Sr$(NO_3)_2$ on a 0.2-mm-thick Ta backing foil. It is worth noting that Ta is provided commercially with some amount of impurities including mainly ^{19}F. As a result, peaks from the ^{19}F$(p,\alpha\gamma)^{16}$O are also observed in the spectrum shown in Fig. 3.

It is finally worth mentioning that the use of a large-volume summing crystal, like the one employed in our work, also takes advantage of the fact that in the vast majority of capture reactions, the resulting sum peak appears at energies considerably higher than the Q values of the disturbing (p,n) and especially (α,n) reactions, which may overload the spectra with a high beam-induced background. The sum peak of interest is, thus, located at the "end" of the spectrum as shown in Fig. 3 and "sits" on a relatively low background.

III. THE EXPERIMENTAL SETUP

The present work was carried out with the 4π calorimeter installed at the Dynamitron Tandem Laboratorium (DTL) of the Ruhr-Universität Bochum, Germany. As shown in Fig. 4, the setup consisted of a 12 × 12 inch NaI(Tl) detector (BICRON) with a bore hole of diameter 35 mm along its axis. The solid angle covered by this detector for photons emitted at its center is almost 98% of 4π. The NaI(Tl) crystal is equipped with six photomultipliers (PM) for the accumulation of the fluorescence light. The resulting signals from the six PMs were first gain matched by appropriate high-voltage settings and then summed. The sum signal was fed into a spectroscopy amplifier. The energy resolution of the detector was ≈2% at ≈10 MeV.

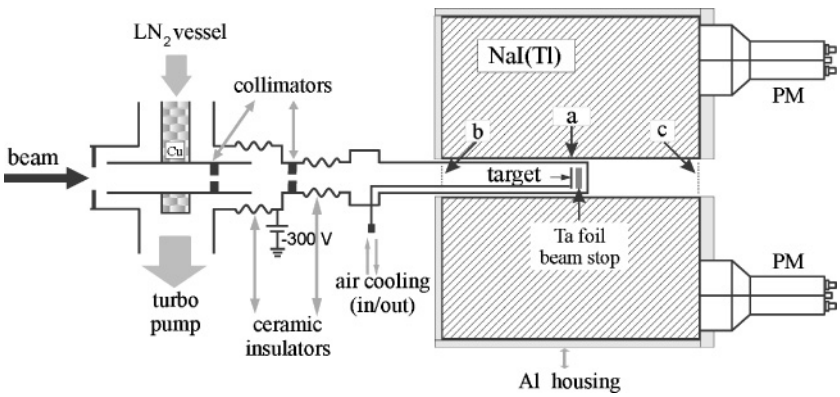

FIG. 4. Layout of the experimental setup used in the present work. The arrows marked with "a," "b," and "c" indicate target positions that are explained in Sec. IV.

As shown in Fig. 4, the beam axis was defined by two Ta collimators having a diameter of 2 and 3 mm, respectively. The former was located at a distance of 1.85 m from the target, whereas the distance of the latter was 0.65 m. The resulting beam spot on the target had a diameter of ≈2 mm. Both Ta collimators as well as the last part of the beam tube were electrically isolated to optimize beam focusing. In addition, the last part of the beam tube served as a faraday cup. For this purpose, a voltage of −300 V was applied on an insulated stainless steel flange, as shown in Fig. 4, to suppress secondary electrons. The beam was stopped at the end of the beam tube by a thick Ta foil.

A high vacuum of $\approx 1 \times 10^{-7}$ mbar was achieved by means of a turbo molecular pump combined with a cool trap, as shown in Fig. 4. Under these conditions no carbon buildup was observed on the targets, which were placed at the center of the detector's bore hole. The targets were mounted on a Ta holder and were cooled with air by means of a couple of stainless steel pipes (Ø3 mm) that were welded on the holder.

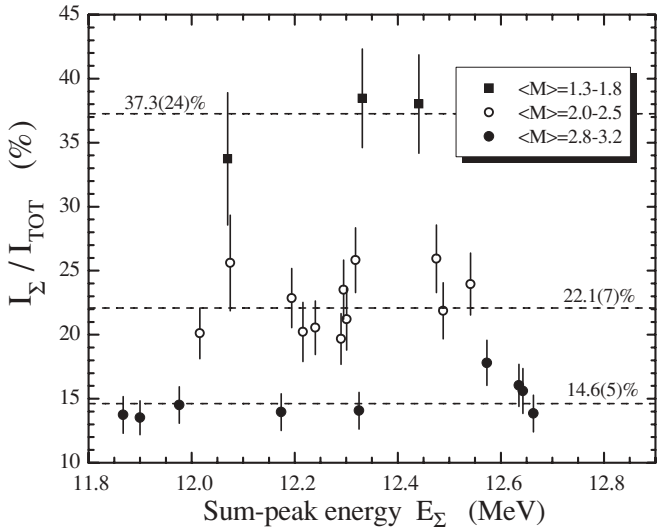

FIG. 5. Ratio of the sum-peak intensity I_Σ to the total intensity I_{TOT} measured [6] for 12 well-known resonances of the $^{27}\mathrm{Al}(p,\gamma)^{28}\mathrm{Si}$ reaction with the 4π summing detector of the present work (see also text).

IV. EXPERIMENTAL PROCEDURES

According to Eq. (3), the main task in the 4π γ-summing technique is the measurement of the sum-peak intensity I_Σ. Then, the total reaction yield Y is obtained from Eq. (3) provided that the sum-peak efficiency ε_Σ is either known or can be determined. However, the latter task is not a trivial one, because ε_Σ can vary strongly with the (mostly unknown) multiplicity M of the various γ cascades, i.e., the number of sequential photons de-exciting the nucleus to the ground state that are "summed" by the detector.

The same 4π summing detector employed in the present work has also been used in our previous studies [6] to measure the resonance strengths of 12 different $^{27}\mathrm{Al} + p$ resonances with known γ branchings [7] at beam energies from 0.12 to 1.12 MeV. Using the spectra measured in Ref. [6], it was found that the sum-peak efficiency ε_Σ of the NaI crystal increases with decreasing M. This dependence is strongly reflected in the ratio of the sum-peak intensity I_Σ over the total intensity I_{TOT} measured for the 12 resonances. This ratio is plotted with respect to the corresponding sum-peak energy E_Σ in Fig. 5. As can be seen in this figure, the data points are scattered all over the x-y plane for energies E_Σ within a 0.8-MeV range only. This scattering can be well understood by considering the corresponding *average* multiplicity $\langle M \rangle$ defined as

$$\langle M \rangle = \sum_i B_i M_i \tag{4}$$

where B_i is the *effective cascade branching* of the i-th γ cascade starting from the resonant (entry) state and terminating at the ground state and M_i is the corresponding cascade multiplicity. B_i is furthermore defined as the product of the branchings of all γ transitions participating in the i-th cascade. To illustrate, in the simple case of the capture reaction displayed in Fig. 1, one has four different cascades sorted arbitrarily as follows:

(i) $i = 1$: Emmission of γ_0 only, i.e., $M_1 = 1$ and $B_1 = b_0$.
(ii) $i = 2$: Cascade formed by the γ_1 and $\gamma_{1,0}$ transitions, i.e., $M_2 = 2$ and $B_2 = b_1 \times b_{1,0}$.
(iii) $i = 3$: Cascade formed by the γ_2, $\gamma_{2,1}$, and $\gamma_{1,0}$ transitions, i.e., $M_3 = 3$ and $B_3 = b_2 \times b_{2,1} \times b_{1,0}$.
(iv) $i = 4$: Cascade formed by the γ_2 and $\gamma_{2,0}$ transitions, i.e., $M_4 = 2$ and $B_4 = b_2 \times b_{2,0}$.

By using the γ branchings compiled in Ref. [7], we calculated the average multiplicities $\langle M \rangle$ of the 12 different resonances for which the ratios of the sum-peak intensity to the total intensity are plotted in Fig. 5. The resulting $\langle M \rangle$ values are displayed in the insert of Fig. 5. Apparently, the scattering of the data can be interpreted as the result of different average multiplicities. Thus, solid squares, i.e., the highest ratios (≈37%), correspond to resonances with $\langle M \rangle$ between 1.3 and 1.8, whereas the lowest ratios (≈15%) indicated by solid circles correspond to resonances with $\langle M \rangle = 2.8$–3.2. Resonances with $\langle M \rangle = 2.0$–2.5 have ratios around 22% (open circles).

From the above analysis, it becomes obvious that before employing the 4π γ-summing technique to determine the cross section of a capture reaction, one has to determine in an independent manner the corresponding average multiplicity $\langle M \rangle$ at each beam energy. In the present work we propose an alternative experimental procedure for the determination of the average multiplicity of the γ cascades summed by a large-volume 4π NaI single crystal. With this new approach, hereforth referred to as the *in/out ratio method*, and using the setup presented in the previous section, we were able to determine first the average multiplicities $\langle M \rangle$ of the reactions of interest and then the corresponding sum-peak efficiency ε_Σ with the aid of Monte Carlo simulations. The latter were performed with the GEANT4 code [8].

A. The in/out ratio method

The in/out ratio method is based on the fact that the summing ability of the 4π NaI *single* crystal, and, hence, its sum-peak efficiency ε_Σ, depends on the position of the target with respect to the NaI crystal. To elucidate the basic idea of the method, let us assume that a single γ ray is emitted from a target placed at the center of the NaI crystal, i.e., at the center of its borehole. This position is indicated in Fig. 4 by the arrow marked with "a." In this case, one obtains a γ spectrum containing a peak of a certain intensity, say I^{in}. The same γ ray, if emitted at the edge of the crystal surface, i.e., at the entrance of its borehole as indicated by either arrow "b" or "c" in Fig. 4, would trivially result in a peak having an intensity $I^{\text{out}} = I^{\text{in}}/2$. If we, furthermore, consider a twofold cascade, emitted at the same positions "b" or "c," then the ratio

$$R = \frac{I_\Sigma^{\text{in}}}{I_\Sigma^{\text{out}}} \tag{5}$$

is expected to be $R = 2 \times 2 = 4$. The latter ratio would obviously be $R = 2 \times 2 \times 2 = 8$ and $R = 2 \times 2 \times 2 \times 2 = 16$ for a γ cascade of multiplity $M = 3$ and 4, respectively.

Based on these considerations, one may expect a correlation between the ratio R and the multiplicity M of the form $R = a^M$, which ideally converts to $R = 2^M$ when the aforementioned in/out ratio is determined with a source placed at the "edge" of the NaI crystal, i.e. at positions "b" or "c" shown in Fig. 4. Hence, the in/out ratio can be used to determine the average multiplicity $\langle M \rangle$ of a capture reaction. Once $\langle M \rangle$ is known, then the sum-peak efficiency ε_Σ can be derived from Monte Carlo simulations as described below. This is the basic idea of the in/out ratio method, which was first tested by means of two standard calibrating γ sources of well-known activity, i.e., ^{137}Cs and ^{60}Co.

The tests were performed by positioning each source at various distances d along the axis of the NaI's borehole and taking γ spectra for a fixed time. Two typical ^{60}Co spectra measured at $d = 0$, i.e., at the center of the crystal as indicated by arrow "a" in Fig. 4 as well as at $d = -16.8$ cm, i.e., at distance slightly longer than that indicated by arrow "b, are plotted in Fig. 6 together with the corresponding GEANT-simulated ones. As shown in Fig. 6, the sum peak decreases considerably. However, the simulated spectra are in almost excellent agreement with the measured ones.

Following the aforementioned procedure, we accumulated ^{137}Cs- and ^{60}Co-source spectra at, respectively, 15 and 17 different positions along the borehole's axis. From these spectra, we obtained, for every distance, the sum-peak intensity ratio R defined by Eq. (5). The results shown in Fig. 7 indicate a value of $R = 2$, at a distance $d \approx \pm 15.3$ cm for the case of ^{137}Cs. At the same distance, one reads $R = 4$ for the case of ^{60}Co. Both values match perfectly well with the expected values because in the case of ^{60}Co the emitted γ cascade is a "pure" (99%) $M = 2$ cascade, whereas in the case of ^{137}Cs a single γ ray is emitted ($M = 1$). As shown in Fig. 7, the data are almost perfectly reproduced by the Monte Carlo simulations performed with the GEANT4 code [8].

After having sucessfully checked the validity of the basic idea of the in/out ratio method with pure $M = 1$ and $M = 2$ cases, the next step was to test it with $M > 2$ and, at the same time, to extract an empirical relationship between R and M. To perform this task it was necessary to use resonant capture reactions with very well known branchings and strengths. Because, however, almost none of the well-known resonances have a single ("pure") multiplicity, one, now, has to deal with average multiplicities that are defined by the branchings of the involved γ cascades. The resonances used for this purpose are listed in Table I. Typical γ spectra measured at $d = 0$ and $d = -16.8$ cm for the ^{27}Al + p resonance at $E_p = 1.118$ MeV are shown in Fig. 8.

The in/out ratios R obtained at $d = -16.8$ cm for the investigated resonances are plotted with respect to the average

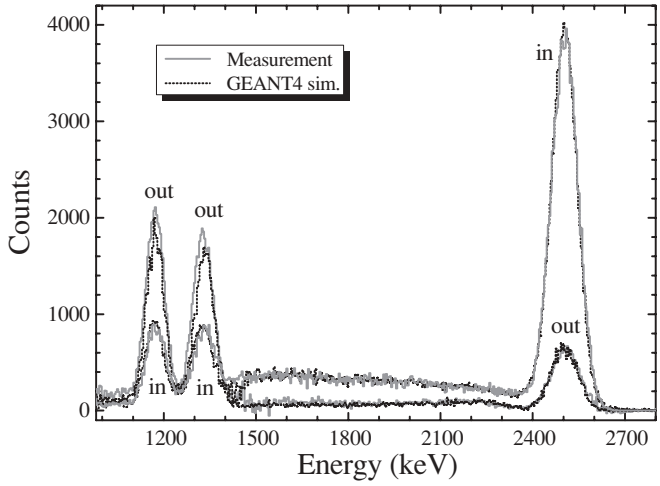

FIG. 6. ^{60}Co-source spectra measured with the 4π NaI summing detector: The spectrum taken by positioning the source at the center of the crystal ($d = 0$ cm) is indicated as "in," whereas that labeled "out" was measured with the source at $d = -16.8$ cm. The dotted spectra are the corresponding GEANT4 simulations.

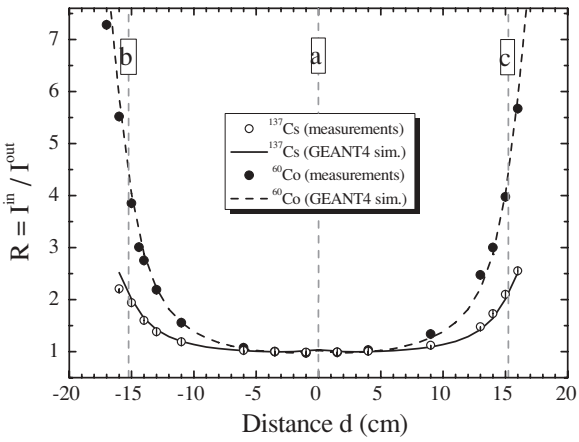

FIG. 7. In/out sum-peak intensity-ratio R measured with a ^{137}Cs source (open circles) and a ^{60}Co source (filled circles) at various distances d along the axis of the NaI's borehole. The solid curves idicate the results of the corresponding GEANT4 simulations. Distance $d = 0$ corresponds to the center of the NaI crystal. The positions indicated by arrows "b" and "c" in Fig. 4 correspond to $d = -15.3$ and $d = +15.3$ cm from the center, respectively.

TABLE I. Resonances used to determine the sum-peak efficiency of the 4π summing detector. The respective target thickness ξ (second column) refers to the specific isotope. The resonance energies given in the third column are laboratory energies. The corresponding resonance strengths and energies of the resonant states are given in the fourth and fifth columns, respectively. The average multiplicities $\langle M\rangle$ (sixth column) were calculated using Eq. (4). The relevant branchings ratios as well as γ strengths and resonance energies were taken from the existing literature (see text). The experimentally determined sum-peak efficiency $\varepsilon_\Sigma^{\rm exp}$ and the corresponding GEANT4-simulated one $\varepsilon_\Sigma^{\rm sim}$ are given in the seventh and eighth column, respectively.

Reaction	ξ (μg/cm^2)	E_R (keV)	$\omega\gamma$ (eV)	E_Σ (keV)	$\langle M\rangle$	$\varepsilon_\Sigma^{\rm exp}$	$\varepsilon_\Sigma^{\rm sim}$
^{26}Mg$(p,\gamma)^{27}$Al	30 ± 2	650	0.105 ± 0.030	8897	1.70	0.216 ± 0.065	0.284
		1249	0.55 ± 0.15	9474	2.25	0.177 ± 0.055	0.197
		1288	1.65 ± 0.40	9511	1.72	0.227 ± 0.061	0.289
		1610	2.45 ± 0.60	9821	2.28	0.178 ± 0.053	0.219
		1966	4.75 ± 0.45	10164	1.49	0.317 ± 0.039	0.293
^{27}Al$(p,\gamma)^{28}$Si	45 ± 3	992	1.94 ± 0.07	12542	2.24	0.155 ± 0.012	0.175
		1118	0.80 ± 0.06	12663	3.22	0.093 ± 0.009	0.095
		1317	0.71 ± 0.12	12854	3.00	0.114 ± 0.021	0.113
^{28}Si$(\alpha,\gamma)^{32}$S	62 ± 6	3738	8.10 ± 1.62	10220	2.87	0.135 ± 0.028	0.143

multiplicities $\langle M\rangle$ in Fig. 9. The latter quantities were calculated using Eq. (4) and the γ-decay branchings given in Refs. [7] and [9] for the ^{27}Al + p resonances, Ref. [10] for ^{26}Mg + p, and Ref. [11] for the ^{28}Si + α resonances. The in/out ratios determined with the ^{137}Cs and ^{60}Co sourses at $d=-16.8$ cm have also been included in Fig. 9 to fit the analytical expression $R=a^{\langle M\rangle}$, with a the adjustable parameter to be determined. From the fitting procedure we obtained $a=2.48\pm0.03$. The resulting best fit curve of the empirical relationship

$$R=2.48(3)^{\langle M\rangle} \tag{6}$$

corresponds to the solid curve shown in Fig. 9 and is characteristic for our setup. This curve can further be used to extract the average multiplicity $\langle M\rangle$ of a capture reaction at a given beam energy by measuring the respective in/out ratio. Once $\langle M\rangle$ is determined, one can derive the corresponding sum-peak efficiency ε_Σ as described in the following section.

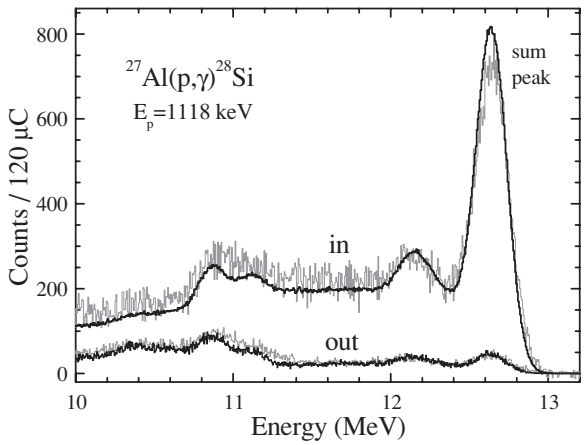

FIG. 8. γ spectra measured at the plateau of the $E_p=1.118$ MeV resonance of the ^{27}Al$(p,\gamma)^{28}$Si reaction. The spectrum labeled "in" was taken with the target placed at the center of the borehole of the NaI crystal ($d=0$), whereas that labeled "out" was measured at $d=-16.8$ cm from the center. This distance corresponds to a slightly longer distance than that indicated by the arrow "b" in Fig. 4. The corresponding GEANT4-simulated spectra are plotted with black bold curves.

B. Determination of the sum-peak efficiency

The sum-peak efficiency ε_Σ of a single summing crystal like the one employed in the present work can be determined by studying resonances of well-known resonance strengths $\omega\gamma$, [12] such as the 992-keV ^{27}Al + p resonance. In such a case, ε_Σ is derived [12] from

$$\omega\gamma=\frac{1}{\varepsilon_\Sigma}\frac{I_\Sigma}{N_b}\frac{2}{\lambda^2}\frac{A}{N_A}\frac{M}{M+m}T(E), \tag{7}$$

where I_Σ is the sum-peak intensity measured for the resonance in consideration, N_b is the number of the beam particles, A is the atomic weight of the target, N_A is the Avogadro number, m and M are the beam and target masses, respectively, λ

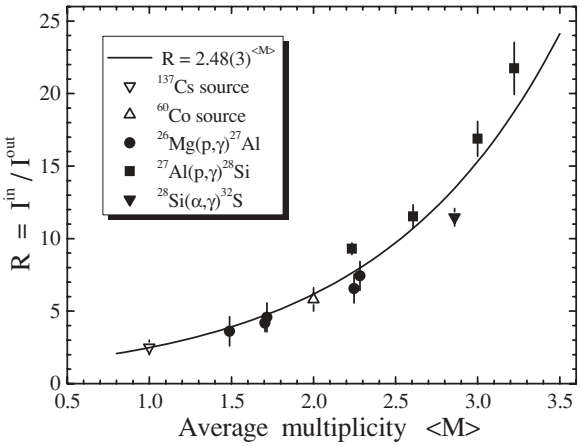

FIG. 9. In/out ratios R determined in the present work for resonances of three capture reactions and two radioactive sources of well-known average multiplicities $\langle M\rangle$. The solid curve corresponds to $R=2.48(3)^{\langle M\rangle}$ obtained by fitting the data (see also text).

is the incident beam wavelength and $T(E)$ is the stopping power of the beam in the target. In addition, when the γ-decay branchings and, hence, the average multiplicities associated with the resonance of interest are known, the sum-peak efficiency can be obtained from Monte Carlo simulations.

In the present work, we first used Eq. (7) for the resonances listed in Table I to determine the corresponding sum-peak efficiencies. The relevant resonance strengths and branching ratios were taken from the existing literature. Hence, the relevant γ branchings and resonance strengths for the ^{26}Mg$(p,\gamma)^{27}$Al reaction were taken from Ref. [10]. These $\omega\gamma$ values are in good agreement with the NACRE-adopted ones [13]. Furthermore, the γ branchings of Ref. [10] are in good agreement within statistical errors with those reported by Ref. [14]. The resonance strengths of the $^{27}\mathrm{Al}+p$ resonances of Table I were taken from Ref. [15]. They are within the reported uncertainties in good agreement with those adopted by NACRE [13] as well as with the ones reported in Ref. [6]. The relevant γ branchings were taken from Ref. [7]. In the case of the ^{28}Si$(\alpha,\gamma)^{32}$S reaction, we adopted the γ branchings and resonance strengths reported in Ref. [16], which agree very well with those reported by Ref. [11]. The stopping powers used in Eq. (7) have been obtained with the code SRIM [17]. Natural targets were used to investigate all the reactions listed in Table I. The target thickness ξ listed in the table refers, however, to the specific isotope. The beam currents varied between 100 and 400 nA. To avoid deterioration effects, all targets were cooled with air during the runs.

Spectra were measured at various beam energies to determine the yield curves of the resonances of interest. Then, spectra with high statistics were measured at beam energies corresponding to the resonance plateaux (=ON spectra) as well as at energies slightly lower than the low-energy edges of the yield curves (=OFF spectra). The OFF spectra were subsequently subtracted from the corresponding ON ones after having been normalized to the same number of beam particles (N_b). The resulting difference spectra were finally used to determine the "net" sum-peak intesities I_Σ of Eq. (7).

The Monte Carlo code GEANT4 [8] was used to simulate the measured resonance spectra and, hence, derive independently the respective sum-peak efficiencies. In the simulations, the geometry of the setup was properly described by means of different volumes corresponding to the NaI crystal, the Al well, the reflective material, the pyrex optical window, the Al housing, the beam tube, the beam stopper, the target itself, and the target holder. The decay paths of the resonant states were described by means of the branchings reported in the aforementioned references. The energies, as well as the γ branchings of the subsequent "secondary" γ transitions were taken from Ref. [18]. Each resonance was simulated by 5×10^5 photons. The GEANT4 code produced a histogram showing the number of the photons versus the energy deposited in the NaI crystal for each resonance. Each histogram was then convoluted with a Gaussian response function to take into account the resolution of the detector at different photon energies. The latter response function was determined from the analysis of the measured spectra. This way a γ spectrum was obtained for every measured resonance and the simulated sum-peak efficiency $\varepsilon_\Sigma^{\mathrm{sim}}$ was derived using

$$\varepsilon_\Sigma^{\mathrm{sim}} = \frac{I_\Sigma^{\mathrm{sim}}}{5\times10^5}, \tag{8}$$

where I_Σ^{sim} is the area under the sum-peak of the GEANT4-simulated γ spectrum. Both the experimentally determined, as well as the simulated sum-peak efficiencies are given in Table I. As can be seen from this table the two different sum-peak efficiency values agree very well. It is worth noting that to achieve this agreement, it was necessary to slightly decrease ($\approx$0.5 inch) the nominal volume (12 $\times$ 12 inch) of the NaI crystal in the GEANT4 simulations. The errors in the experimental sum-peak efficiencies listed in Table I include the uncertainties in the (i) $\omega\gamma$ values (given in this table), (ii) stopping powers ($\approx$5%), and (iii) charge measurement (3%).

In addition to the resonance reactions, GEANT4 simulations were also performed in order to study the dependence of the sum-peak efficiency ε_Σ on $\langle M\rangle$ using again 5×10^5 random events of a specific multiplicity $\langle M\rangle$ and various sum-peak energies E_Σ. Hereby, for a given $\langle M\rangle$, E_Σ was varied from 8 to 16 MeV, with a step of 1 MeV. In addition, various combinations of photon energies resulting in the same sum-peak energy E_Σ were assumed. As a result we obtained ε_Σ values for different sum-peak energies E_Σ and different multiplicities $\langle M\rangle$ ranging from 1 to 7. These simulated sum-peak efficiencies are plotted in Fig. 10 (solid curves) together with the experimental values determined in the present work. The shaded areas correspond to the unceratinties of the simulations for $\langle M\rangle = 2, 3, 5$ due to the different results obtained by arbitrary variation in the energies of the γ rays forming a cascade of given multiplicity and sum-peak energy. Obviously, no uncertainties can be assigned to the simulated sum-peak efficiencies for $\langle M\rangle = 1$. The shaded areas shown in Fig. 10 correspond to relative errors of $\approx$8, 15, and 30% for $\langle M\rangle = 2$, 3, and 5, respectively. For $\langle M\rangle = 4$ the relative uncertainty (not shown in Fig. 10) amounts to $\approx$21%, whereas for multiplicities higher than 5 it exceeds 40%.

According to Fig. 10, the sum-peak efficiency is indeed very sensitive to multiplicity changes. At $E_\Sigma = 12$ MeV, ε_Σ decreases exponentially from $\approx$33% ($M = 1$) down to $\approx$6% ($M = 5$). However, it converges to some constant value of $\approx$3.5% for multiplicities higher than 5. This decrease is clearly shown in Fig. 11. The sum-peak efficiencies (solid circles) derived from Monte Carlo simulations can be fitted very well with a single exponential function (dashed curve). The exponetial decrease shown in Fig. 11 was found to be obeyed by the simulated sum-peak efficincies for all sum-peak energies. From the above analysis it is obvious that is mandatory to first determine the (average) multiplicity of the reaction of interest before applying the 4π summing technique to obtain its cross section.

V. CROSS SECTION MEASUREMENTS

The 4π γ-summing method presented above has been applied to series of 25 cross-section measurements of proton and α-capture reactions in the Ni–Sb region. The targets used in the (p,γ) and (α,γ) reactions investigated are shown in

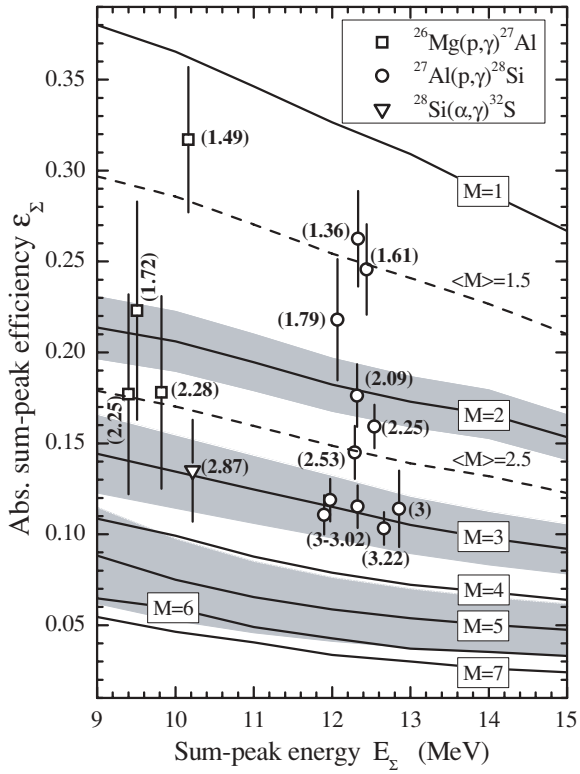

FIG. 10. Experimental and simulated sum peak efficiencies determined in the present work for different sum-peak energies E_Σ and multiplicities $\langle M \rangle$ using the resonances of the three reactions listed in the legend. Numbers in parentheses indicate the average multiplicity of the corresponding resonance. The shaded areas correspond to the uncertainties of the simulations for $\langle M \rangle = 2$, 3, and 5 (see also text).

Fig. 12 with black and gray boxes, respectively. The main goal in the case of the ^{62}Ni$(\alpha, \gamma)^{66}$Zn reaction was to mainly test the reliability of our method because the cross section of this reaction is very well known from the previous work reported in Ref. [19]. In this article, we present the cross

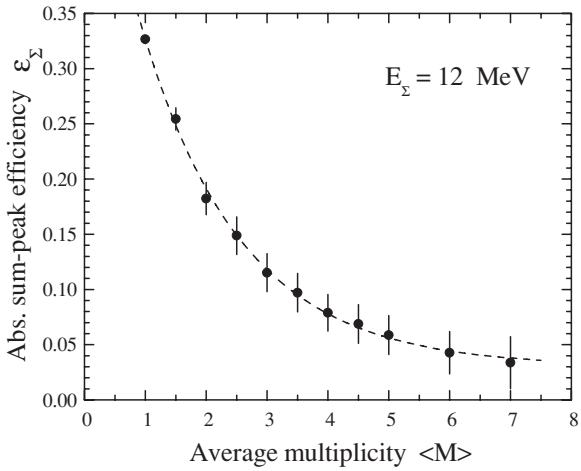

FIG. 11. Sum-peak efficincies (black circles) of a 12-MeV sum peak obtained from Monte Carlo simulations for various average multiplicities. The dashed curve corresponds to a single-exponential function fit.

sections we obtained for the ^{62}Ni$(\alpha, \gamma)^{66}$Zn reaction as well as for ^{103}Rh$(p, \gamma)^{104}$Pd.

The cross section of the ^{62}Ni$(\alpha, \gamma)^{66}$Zn reaction was measured by Zyskind *et al.* [19] using in-beam high-resolution spectroscopy, a 280-μg/cm^2-thick ^{62}Ni target backed with a Ta foil and a Ge(Li) detector placed at 55° with respect to the beam direction. In our experiment, we used a 98%-enriched self-supporting ^{62}Ni target with 413±29 μg/cm^2 thickness that corresponds to an energy loss in the target of $\Delta E \approx 178$ and ≈124 keV at beam energies of 5 and 9 MeV, respectively. The target thickness was determined from Rutherford Backscattering (RBS) measurements and was found to be (within statistical errors) in very good agreement with the result of an independent XRF measurement.

The current of the α-beam on target ranged from 6 to 140 nA depending on the dead time. Accordingly, the accumulated total charge varied from 6 to 240 μC. The ^{62}Ni target was cooled with air during all runs. No target deterioration effects were found after the measurements. It is worth noting that air cooling was used in all measurements performed with the 4π technique.

For the ^{103}Rh$(p, \gamma)^{104}$Pd reaction no data exist in the literature. Therefore, this is the first time this reaction is measured. In our experiment, we used a ^{103}Rh target produced by evaporating high-pure (>99.999) natural Rh on a 0.2-mm-thick Ta foil. The thickness of the ^{103}Rh target was determined by the XRF technique and was found to be 161±10 μg/cm^2, which corresponds to energy losses in the target of $\Delta E \approx 8$ and ≈6 keV at proton-beam energies of 3 and 5 MeV, respectively. The current of the proton beam ranged between 10 and 100 nA. The ^{103}Rh target was checked again using XRF after the experiment and was found to be stable within 3%.

Gamma "in" and "out" spectra were measured at different beam energies as described in the previous sections. The "in" and "out" spectra obtained at 6.5 MeV for the ^{62}Ni$(\alpha, \gamma)^{66}$Zn reaction are plotted in Fig. 13. The in/out ratios R determined from the "in" and "out" spectra were used to derive average multiplicities $\langle M \rangle$ from Eq. (6). Sum peak efficiencies were subsequently determined for every $\langle M \rangle$ as described in the previous section. Cross sections were finally determined by applying Eqs. (3) and (1).

The results for the average multiplicities $\langle M \rangle$ of ^{62}Ni$(\alpha, \gamma)^{66}$Zn are plotted in the upper panel of Fig. 14 (solid squares). As can be seen, $\langle M \rangle$ increases with increasing sum-peak energy, i.e., the excitation energy of the produced compound nucleus, and in this particular case it varies between 2.5 and 3.5. Similar values of $\langle M \rangle$ were obtained for most of the reactions investigated in our work that lead to the formation of an even-even compound nucleus, and the results for the ^{92}Mo$(\alpha, \gamma)^{96}$Ru and ^{103}Rh$(p, \gamma)^{104}$Pd cases are displayed in Fig. 14 (open squares and open down-triangles, respectively). Also shown in this figure are the typical average multiplicities ($\langle M \rangle$ between 4 and 4.5) obtained for the ^{105}Pd$(p, \gamma)^{106}$Ag reaction producing an odd-odd compound system (solid up-triangles).

According to the same figure, for the ^{104}Pd$(p, \gamma)^{105}$Ag and ^{118}Sn$(p, \gamma)^{119}$Sb reactions leading to the formation of an odd-even compound nucleus, the values of $\langle M \rangle$ (open and solid circles, respectively) are higher than those obtained for

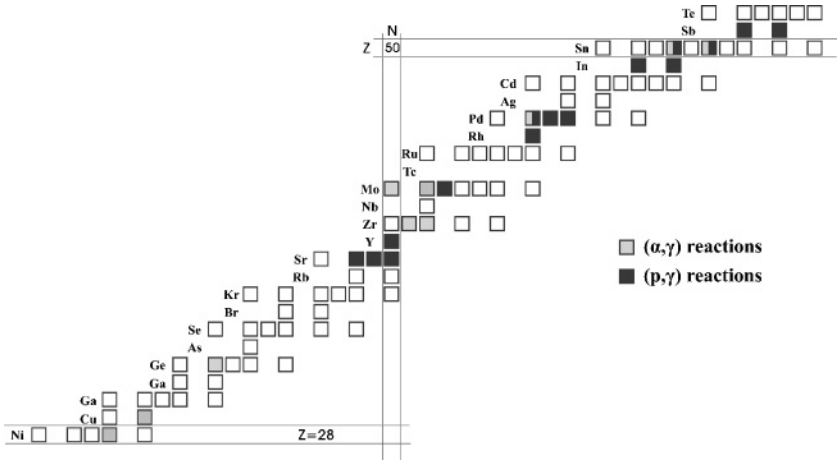

FIG. 12. Stable isotopes used so far in cross section measurements of (α, γ) reactions (gray boxes) and (p, γ) reactions (black boxes) carried out by employing the 4π γ-summing method.

even-even compound nuclei and lower than those for odd-odd compound nuclei at similar excitation (sum-peak) energies. Very similar average multiplicities like those of the latter two (p, γ) reactions were obtained in our systematics for all other (p, γ) reactions producing an odd-even compound nucleus. The differences in $\langle M \rangle$ shown in Fig. 14 most probably reflect the influence of pairing. As such they are expected to vanish with increasing excitation energy. The data seem to suggest such a trend at excitation energies above $\approx$11.5 MeV.

The average multiplicities shown in Fig. 14 (top panel) were used to extract the corresponding sum-peak efficiencies. For this task the Monte Carlo simulated efficiencies shown in Fig. 10 (solid curves) were employed. The following convention was hereby adopted: for a given average multiplicity of decimal form X.yz, (e.g, 2.48) the corresponding $\langle M \rangle$ value reads

$$\varepsilon_{\langle M \rangle} = (1 - 0.yz) \times \varepsilon_{M=X} + 0.yz \times \varepsilon_{M=X+1}. \quad (9)$$

Hence, for $\langle M \rangle = 2.48$, one obtains $\varepsilon = 0.52 \times \varepsilon_{M=2} + 0.48 \times \varepsilon_{M=3}$. Obviously, one may find a number of arbitrary

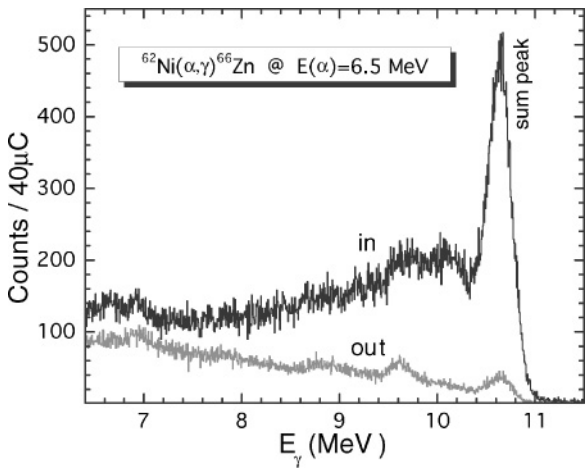

FIG. 13. γ spectra of the ^{62}Ni$(\alpha, \gamma)^{66}$Zn reaction measured at $E(\alpha) = 6.5$ MeV. The spectrum labeled "in" was taken with the target at the center of the NaI crystal ($d = 0$) as indicated by the arrow "a" in Fig. 4, whereas that labeled "out" was measured at $d = -16.8$ cm from the center. This distance correspond to a slightly longer distance than that indicated by the arrow "b" in Fig. 4.

combinations of efficiencies at different multiplicities that give the corresponding efficiency at $\langle M \rangle$. However, the convention applied here is transparent and straightforward, in contrast to other methods that may use non-realistic multiplicity combinations.

The resulting sum-peak efficiencies $\varepsilon_{\langle M \rangle}$ are shown in Fig. 14 (bottom panel). The solid and dashed curves correspond to single exponential fits to the sum-peak efficiencies obtained for capture reactions leading to even-even and odd-even compound nuclei, respectively. In Fig. 14 one observes that

(i) the sum-peak efficiency decreases with increasing sum-peak energy. This decrease can be quite satisfactorily described by a single exponential function of the form $\varepsilon_\Sigma = \varepsilon_0 + a \times \exp(-E_\Sigma/b)$.
(ii) the sum-peak efficiency decrease is sharper in the case of capture reactions producing even-even compound nuclei than in the cases where odd mass compound systems are formed.
(iii) for sum-peak energies above $\approx$12 MeV the sum-peak efficiency is almost constant, i.e., $\approx$0.07–0.08.
(iv) in the energy region investigated, the efficiency of the sum peak in capture reactions producing odd-odd compound nuclei can be described by Monte Carlo simulations with $M = 4$, with an accuracy of $\approx$20–25%.

The cross sections obtained in the present work are listed in Table II. The center-of-mass energies given in the first and third column of this table are the effective beam energies E_{eff} in the center-of-mass system. These were obtained from

$$E_{\text{eff}} = E_{\text{beam}} - \frac{\Delta E}{2}, \quad (10)$$

where E_{beam} is the beam energy and ΔE the corresponding target thickness. The latter were derived using appropriate stopping powers [17]. The cross sections of the reactions ^{62}Ni$(\alpha, \gamma)^{66}$Zn and ^{103}Rh$(p, \gamma)^{104}$Pd are plotted in Fig. 15 and 16 (black circles), respectively. Also included in Fig. 15 are the data of Ref. [19] (open circles). As can be seen, the two sets of measurements are in excellent agreement.

The data are also compared with predictions of the Hauser-Feshbach (HF) theory. A key factor in the description of the

TABLE II. Total cross sections σ_T measured in the present work for the reactions ^{62}Ni$(\alpha,\gamma)^{66}$Zn (second column) and ^{103}Rh$(p,\gamma)^{104}$Pd (fourth column). The corresponding center-of-mass energies are given in the first and third columns, respectively.

^{62}Ni$(\alpha,\gamma)^{66}$Zn		^{103}Rh$(p,\gamma)^{104}$Pd	
$E_{\text{c.m.}}$ (MeV)	σ_T (μb)	$E_{\text{c.m.}}$ (MeV)	σ_T (μb)
4.613	2.5 ± 0.5	2.967	5.5 ± 1.0
5.086	18.1 ± 3.4	3.165	8.6 ± 1.6
6.034	318 ± 60	3.462	16.8 ± 3.1
6.318	547 ± 102	3.561	22.4 ± 4.1
6.412	598 ± 111	3.760	28.8 ± 5.3
6.507	527 ± 98	3.958	42.1 ± 7.8
6.791	223 ± 41	4.156	65.2 ± 11.9
7.263	287 ± 53	4.354	75.4 ± 13.8
7.735	277 ± 51	4.552	126 ± 23
8.395	400 ± 75	4.750	120 ± 22
		4.949	165 ± 30

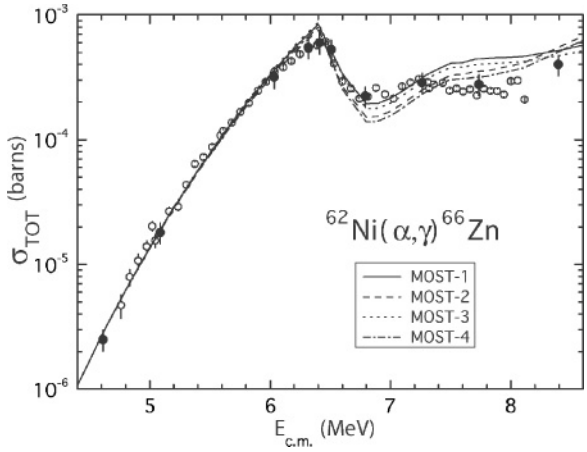

FIG. 15. Cross sections (solid circles) obtained in the present work for the ^{62}Ni$(\alpha,\gamma)^{66}$Zn reaction compared with those reported in Ref. [19] (open circles) as well as with HF predictions (curves).

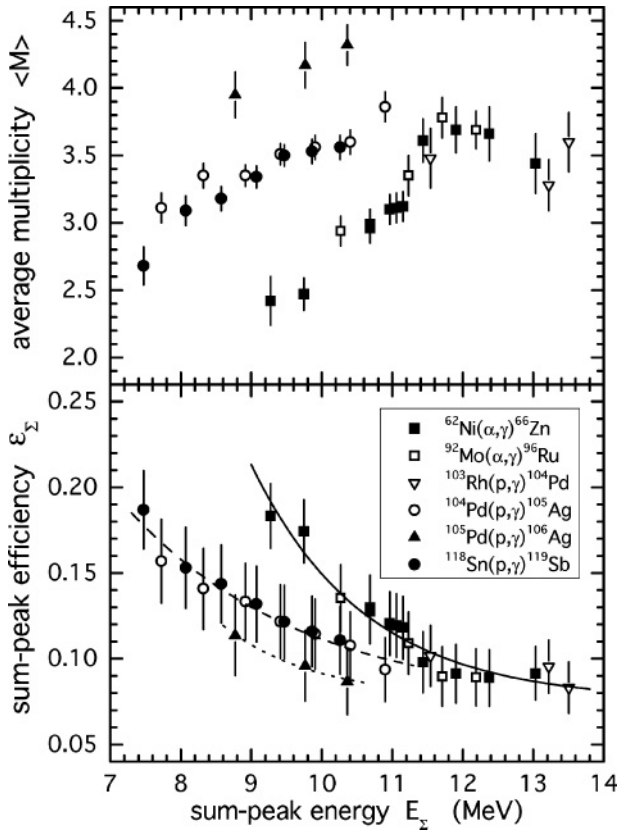

FIG. 14. (Top panel) Average multiplicities $\langle M \rangle$ resulted from the ratios R measured in our work for various capture reactions and using the empirically determined relation $R = 2.48(3)^{\langle M \rangle}$ (Eq. (6) and Fig. 9). (Bottom panel) Sum-peak efficiencies obtained for the corresponding sum-peak energies of the capture reactions included in the top panel. The solid and dashed curves indicate fits of a single exponential function to the data corresponding to the reactions producing an even-even and odd-even compound nucleus, respectively (see also text).

entrance channel in the HF formalism, is the α-nucleus optical model potential (OMP), which is rather poorly known at low energies near the Coulomb barrier. In the present work, we use the global semimicroscopic α OMP of Demetriou *et al.* [20]. This potential (OMP III of Ref. [20]) consists of a real part obtained from the double-folding method using a realistic nucleon-nucleon interaction, and a phenomenological imaginary part that includes both volume and surface absorption described by Woods-Saxon functionals. Dispersive corrections have also considered in OMP III. The depth and geometry of the imaginary potential have been adjusted to reproduce all existing low-energy scattering and reaction data involving α-particles, hence the global nature of the OMP.

Apart from the α-nucleus OMP, other ingredients of the HF calculations can also have an impact on the cross sections. As soon as the neutron and proton emission channels open, the HF cross section will also depend strongly on the nucleon OMPs and the nuclear level densities (NLD) of the residual nuclei in the respective exit channels. To test the sensitivity of the predictions to the above-mentioned nuclear properties, we have performed HF calculations with the statistical model code MOST [21] using four different combinations of nucleon OMPs and NLDs labeled MOST-1, MOST-2, MOST-3, and MOST-4. In the former two combinations, we used the microscopic nucleon-nucleus OMP of Jeukenne *et al.* [22] with (i) the microscopic NLDs of Demetriou and Goriely [23] (MOST-1) and (ii) the phenomenological NLDs of Thielemann *et al.* [24] (MOST-2). The latter two predictions, i.e., MOST-3 and MOST-4, combined the phenomenological nucleon-nucleus OMP of Koning and Delaroche [25] with the aforementioned NLDs of Refs. [23] and [24], respectively.

Other nuclear input to the statistical model code include (i) nuclear masses, (ii) ground state properties (matter density, single-particle level scheme), and (iii) γ-ray strength functions. In this work, the input parameters used for quantities (i) and (ii) were taken from Refs. [26] and [27], respectively. For the $E1$ and $M1$ strength functions we adopted the hybrid model of Ref. [28] and the parametrization of Ref. [29], respectively.

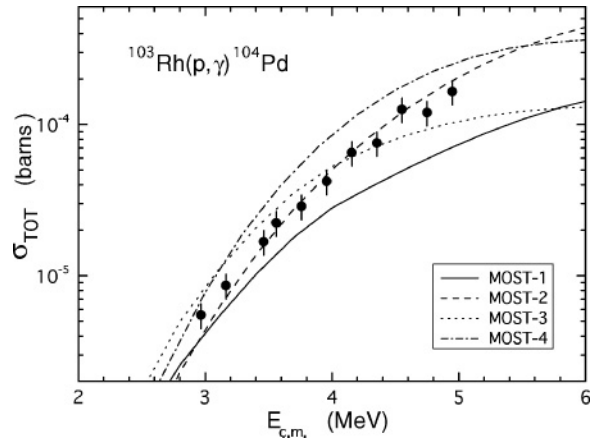

FIG. 16. Cross sections (solid circles) obtained in the present work for the ^{103}Rh$(p,\gamma)^{104}$Pd reaction compared with HF predictions (curves).

The results of the calculations for the ^{62}Ni$(\alpha,\gamma)^{66}$Zn reaction are shown in Fig. 15. As can be seen, below the neutron threshold (6.4 MeV) all four combinations converge because the cross sections depend only on the α OMP. Apparently, the α OMP of Ref. [20] gives a very good description of the data. Above the neutron threshold of 6.4 MeV, the different nucleon OMPs and NLDs come into play and the four curves deviate. The best overall agreement is obtained with MOST-2 and MOST-4.

The results for ^{103}Rh$(p,\gamma)^{104}$Pd are shown in Fig. 16. In this case, the (p,n) channel opens at the fairly low energy of $\approx$1.33 MeV. As a result, the HF calculations are very sensitive not only to the nucleon-nucleus OMP but also to the NLDs in the exit channels throughout the entire energy region covered by our measurements. From the comparison in Fig. 16, it appears that the data show a preference for combination MOST-2.

VI. CONCLUSIONS

In the present work, a 4π γ-summing technique capable of measuring cross sections of proton and α-particle capture reactions on medium-mass nuclei has been developed. It can provide total cross sections with an average uncertainty between 10 and 20%. As shown in Sec. IV, this accuracy reflects mainly the uncertainties in the sum-peak efficiency due to its strong dependence on the average multiplicity of the reaction of interest. In the present work, we have developed for the first time a simple experimental procedure, called the in/out ratio method, to determine average multiplicities of capture reactions producing compound nuclei at excited states in the continuum phase space.

The method proposed was first applied to the ^{62}Ni$(\alpha,\gamma)^{66}$Zn reaction, which has been measured before [19] and therefore has well-known cross sections. Subsequently, we performed a series of cross-section measurements of 15 (p,γ) and 10 (α,γ) reactions. In this article we report only on the measurements of the ^{62}Ni$(\alpha,\gamma)^{66}$Zn and ^{103}Rh$(p,\gamma)^{104}$Pd reactions. The results of the remaining reactions will be the subject of forthcoming publications.

The new data have also been compared with Hauser-Feshbach (HF) calculations. The (α,γ) cross sections are well reproduced with the α-OMP-III of Demetriou *et al.* [20]. Similar agreement has also been observed in most of the other α-capture reactions included in our systematics. However, the (p,γ) cross sections are best described by the microscopic nucleon-nucleus OMP of Jeukenne *et al.* [22] combined with the phenomenological NLD of Thielemann *et al.* [24]. The latter combination gives good agreement in some of the other (p,γ) reactions investigated. Nevertheless, we have still not arrived at a global combination of input parameters that could be recommended for any radiative capture reaction.

ACKNOWLEDGMENTS

The authors thank Dr. P. Demetriou for providing us with the HF calculations and for useful discussions. This work was supported by the Hellenic State Scholarship Foundation (IKY), the German Academic Exchange Service (DAAD), and the Dynamitron-Tandem-Laboratorium (DTL) of the University of Bochum.

[1] T. Sauter and F. Kappeler, Phys. Rev. C **55**, 3127 (1997).
[2] S. Galanopoulos, P. Demetriou, M. Kokkoris, S. Harissopulos, R. Kunz, M. Fey, J. W. Hammer, G. Gyürky, Zs. Fülop, E. Somorjai, and S. Goriely, Phys. Rev. C **67**, 015801 (2003).
[3] S. Harissopulos, E. Skreti, P. Tsagari, G. Souliotis, P. Demetriou, T. Paradellis, J. W. Hammer, R. Kunz, C. Angulo, S. Goriely, and T. Rauscher, Phys. Rev. C **64**, 055804 (2001).
[4] M. Arnould and S. Goriely, Phys. Rep. **384**, 1 (2003).
[5] P. Tsagari, M. Kokkoris, E. Skreti, A. G. Karydas, S. Harissopulos, T. Paradellis, and P. Demetriou, Phys. Rev. C **70**, 015802 (2004).
[6] S. Harissopulos, C. Chronidou, K. Spyrou, T. Paradellis, C. Rolfs, W. H. Schulte, and H. W. Becker, Eur. Phys. J. A **9**, 479 (2000).
[7] M. A. Meyer, I. Venter, and D. Reitmann, Nucl. Phys. **A250**, 235 (1975).
[8] GEANT4: A Simulation Toolkit, S. Agostinelli *et al.*, Nucl. Instrum. Methods A **506**, 250 (2003).
[9] A. Anttila, J. Keinonen, M. Hautala, and I. Forsblom, Nucl. Instrum. Methods **147**, 501 (1977), and references therein.
[10] J. J. A. Smit, J. P. L. Reinecke, M. A. Meyer, D. Reitmann, and P. M. Endt, Nucl. Phys. **A377**, 15 (1982).
[11] J. Vernotte, M. Langevin, S. Fortier, E. Bozek, A. Chevallier, A. J. Pape, and J. C. Sens, Nucl. Phys. **A124**, 350 (1969).
[12] C. E. Rolfs and W. S. Rodney, *Cauldrons in the Cosmos* (The University of Chicago Press, Chicago, 1988).
[13] C. Angulo, M. Arnould, M. Rayet, P. Descouvemont, D. Baye, C. Leclerq-Willain, A. Coc, S. Barhoumi, P. Auger, C. Rolfs, R. Kunz, J. W. Hammer, A. Mayer, T. Paradellis, S. Kossionides, C. Chronidou, K. Spyrou, S. Degl'Innocenti, G. Fiorentini, B. Ricci, S. Zavaratelli, C. Providencia, H. Wolters, J. Soares,

C. Grama, J. Rahighi, A. Shotter, and M. Lamehi Rachti, Nucl. Phys. **A656**, 3 (1999).
[14] J. Keinonen and S. Brandenbourg, Nucl. Phys. **A341**, 345 (1980).
[15] C. Chronidou, K. Spyrou, S. Harissopulos, S. Kossionides, and T. Paradellis, Eur. Phys. J. A **6**, 303 (1999).
[16] D. W. O. Rogers, W. R. Dixon, and R. S. Storey, Nucl. Phys. **A281**, 345 (1977).
[17] J. F. Ziegler and J. P. Biersack, Code SRIM Version 2003. Full description given by J. F. Ziegler, J. P. Biersack, and U. Littmark, *The Stopping and Range of Ions in Solids* (Pergamon, New York, 1985).
[18] R. B. Firestone, V. S. Shirley, C. M. Baglin, J. Zipkin, and S. Y. F. Chu, *Table of Isotopes*, 8th ed. (Wiley-Interscience, New York, 1996).
[19] J. L. Zyskind, J. M. Davidson, M. T. Esat, M. H. Shapiro, and R. H. Spear, Nucl. Phys. **A331**, 180 (1979).
[20] P. Demetriou, C. Grama, and S. Goriely, Nucl. Phys. **A707**, 141 (2002).
[21] S. Goriely, in *Nuclei in the Cosmos V*, edited by N. Prantzos and S. Harissopulos (Editions Frontières, Paris, 1998), p. 314 (see also in http://www-astro.ulb.ac.be).
[22] J. P. Jeukenne, A. Lejeune, and C. Mahaux, Phys. Rev. C **16**, 80 (1977).
[23] P. Demetriou and S. Goriely, Nucl. Phys. **A695**, 95 (2001).
[24] F.-K. Thielemann, M. Arnould, and J. W. Truran, in *Advances in Nuclear Astrophysics*, edited by E. Vangioni-Flam, J. Audouze, M. Cassé, J.-P. Chieze, and J. Tran Thanh Van (Editions Frontières, Gif-sur-Yvette, 1986), p. 525.
[25] A. Koning and J. P. Delaroche, Nucl. Phys. **A713**, 231 (2003).
[26] G. Audi and A. H. Wapstra, Nucl. Phys. **A595**, 409 (1995).
[27] S. Goriely, F. Tondeur, and J. M. Pearson, At. Data Nucl. Data Tables **77**, 311 (2001).
[28] S. Goriely, Phys. Lett. **B436**, 10 (1998).
[29] J. Kopecky and R. E. Chrien, Nucl. Phys. **A468**, 285 (1987).